Bulletin of Mathematical Biology (2006) 68: 1819–1836
DOI 10.1007/s11538-006-9071-2

ORIGINAL ARTICLE

Mechanics and Chemotaxis in the Morphogenesis of Vascular Networks

A. Tosin*, D. Ambrosi, L. Preziosi

Politecnico di Torino, Dipartimento di Matematica
Corso Duca degli Abruzzi 24-10129 Torino, Italy

Received: 18 March 2005 / Accepted: 20 October 2005 / Published online: 1 July 2006

Abstract The formation of vascular networks in vitro develops along two rather distinct stages: during the early migration-dominated stage the main features of the pattern emerge, later the mechanical interaction of the cells with the substratum stretches the network. Mathematical models in the relevant literature have been focusing just on either of the aspects of this complex system. In this paper, a unified view of the morphogenetic process is provided in terms of physical mechanisms and mathematical modeling.

Keywords Vascular networks · Vasculogenesis · Chemotaxis · Cell traction · Elasticity

1. Introduction

When cultured in vitro in a suitable environment, endothelial cells (ECs) are able to organize themselves to form capillary-like networks. This characteristic is shared by several cell lines (Vailhe et al., 2001); particularly interesting is the observation that also melanoma cells seem to have the capability to form capillary-like structures by themselves, which favor their growth (Hendrix et al., 2001; Mariotis et al., 1999). The details of the morphogenetic process may differ depending on the specific experimental setting at hand (see Ambrosi et al., 2005 for an extended review on this issue).

Mathematical literature on the subject is quite partitioned into two mainstreams, that in essence correspond to two different explanations for the basic mechanism of intercellular communication leading to pattern formation. The earlier thread is due to Murray, Oster, and coworkers (see Murray and Oster, 1984 and other papers referenced therein; Manoussaki et al., 1996). They focus on the mechanical

*Corresponding author.
E-mail addresses: andrea.tosin@polito.it (A. Tosin), davide.ambrosi@polito.it (D. Ambrosi), luigi.preziosi@polito.it (L. Preziosi).

interactions between cells and extracellular matrix (ECM) that occur when ECs adhere to the underlying layer and stretch it. These authors observe that the tensional field caused by the cell pulling on the substratum creates a local indirect information about the concentration of the cells themselves on the surrounding surface. They therefore assume that ECs detect the stress field of the layer and move on the surface along the tensional lines (*mesenchymal motion*). Cell organization in soft media due to active mechanosensing has been confirmed by a number of experiments reported in the recent literature too (see Bischofs and Schwartz, 2003 and the references therein). As the tension depends on the number of pulling cells, the migrating ones move toward regions of larger cellular density. Qualitative analysis and numerical integration of the set of partial differential equations corresponding to the mathematical formalization of this idea demonstrate that network-like structures actually form on the basis of this assumption.

However, recent experimental works (Serini et al., 2003) have pointed out that before mesenchymal motion activates cells undergo a faster *amoeboid-type migration* driven by chemical factors such as Vascular Endothelial Growth Factor (VEGF). During this stage, a draft of the final network emerges, although it exhibits itself in the final form only after the stretching process. Even more important, laboratory investigations demonstrate that a characteristic mesh size independent of the number of cells exists, provided the latter are neither too many nor too few in order for the morphogenetic process to start up. Conversely, the conjecture that the network forms just during the mesenchymal migration does not predict the existence of any characteristic length, so that the final mesh size would be dictated essentially by the initial conditions. The key role of the VEGF in network formation is also demonstrated by the experiment of Helmlinger et al. (2000). They study the network-like structures formed by human umbilical cells in a sandwich, where the stretching of the substratum is inhibited. The morphology of the pictures in their paper exhibits a characteristic length, but the cords are quite thicker and less rectilinear than in usual ECM assays (see e.g., Tranqui and Tracqui, 2000; Vailhe et al., 2001; Namy et al., 2004), thus suggesting again the fundamental role of chemical intercellular communication in this process.

To obviate these difficulties of theory, some authors have recently proposed mathematical models in which the chemotactic interaction is the real driver of network formation (Ambrosi et al., 2004; Gamba et al., 2003). This assumption is supported by the observation that exogenous saturation of the signaling of some VEGF inhibits the networking. The mathematical model identifying the chemical signaling as the key mechanism of vasculogenesis predicts a characteristic length of the mesh size, which is in good agreement with the experiments.

Aim of this paper is to provide a unified view of the whole morphogenetic process of vascular networks, including both amoeboid and mesenchymal migration. ECs and ECM are described as a two-layers system in which the vertical dimension can be neglected. The two layers are shallow continuous bodies that obey standard force balance equations including an interaction term, which couples the motion of the cells and the substratum. This simple setting allows to include in the description both the (independent) reorganization of the cells according to chemotactic signaling and the (coupled) stretching of the gel. This approach provides a satisfactory unified framework for the vasculogenic process at all stages, and the

numerical simulations suggest that a stable steady solution should exist in a physically significant range of parameters.

This paper is divided into six sections. After this Introduction, Section 2 is devoted to summarize the experimental facts of a particular biological assay, while in Section 3 a new mathematical model is illustrated accounting for both chemotactic and mechanical aspects of the vasculogenic process. This model is discussed and compared with the existing ones in Section 4, and in Section 5 the results of the related numerical simulations are shown and commented. Finally, Section 6 briefly sketches some research perspectives.

2. Experimental facts

In this section, we specifically refer to the experiments by Serini et al. (2003). Generalization of the dynamics illustrated here to other vasculogenesis assays (involving different cells or different substrata) should be done with great care.

Serini and his coworkers use a Petri dish coated with an amount of Matrigel, a surface that favors cell motility thanks to biochemical characteristics similar to those of living tissues. Human ECs from large veins (e.g., HUVEC, Human Umbilical Vein ECs) or from adrenal cortex capillaries are dispersed in a physiological solution, which is poured on the top of the Matrigel. After sedimentation due to gravity, cells move on the horizontal surface of the substratum giving rise to a process of aggregation and pattern formation.

If the proper number of cells is used (cell density ranging from 100 to 400 cell/mm^2), a vascular-like network develops. The entire process lasts 12–15 h and evolves according to the following steps:

(i) in the first few hours (2–3 h) ECs migrate independently, keeping a round shape (Fig. 1a–b). In this phase, cell motion is of amoeboid type (see e.g., Friedl and Wolf, 2003; Webb and Horwitz, 2003; Wolf et al., 2003); it is faster than later motion and shows a high persistence (Serini et al., 2003; Sambeth and Bamgaertner, 2001). Intriguingly, an indirect confirmation of the existence of this amoeboid stage can be deduced also from the experiment of Ferrenq et al. (1997): they measure the traction exerted by the cells on the gel, and almost no action is registered in the first 2 h, a stage that they call "latency time" and that can probably be interpreted in terms of amoeboid motion;

(ii) the cells, attracted toward regions with higher cellular density, attach to the neighboring ones and, if possible, form a continuous multicellular network (Fig. 1c);

(iii) the cells take a more elongated shape. Their motion becomes mesenchymal, they anchor themselves to the ECM, and, acting on the adhesion sites, start pulling the substratum and the other cells. The network slowly moves as a whole, undergoing a slow thinning process (Fig. 1d), probably driven by the stress field generated by mutual tractions;

(iv) in the final phase, individual cells differentiate and fold up to form the lumen of the capillaries, so that the formation of a capillary-like network takes

place along the lines of the previously formed two-dimensional structure as described in Grant et al. (1989) and Kubota et al. (1988).

A movie of an experiment can be viewed at the EMBO web site[1] as a supplementary material to the paper by Serini et al. (2003).

Two transitions are observed at low and high cell densities. The former is a percolative transition that occurs below the critical threshold of 100 cells/mm^2 and gives rise to groups of disconnected structures. This transition is analyzed in detail in Gamba et al. (2003). The latter gives rise to thicker cords, and for very high cell density (say above 400 cells/mm^2) to the formation of a continuous carpet of cells with holes or *lacunae*.

Note that the experimental evidences reported in the Introduction demonstrate the role of the chemotactic interaction in pattern generation, but there is no reason to restrict this effect to the amoeboid stage; it seems instead reasonable that also the apparent mesh remodeling occurring at later times be driven by a joint chemomechanical interaction.

3. The two-layers model

In our mathematical model deduction, we regard ECs and ECM as two continuous shallow layers. In the experiments, the substratum has a horizontal length of the order of 1 mm, and a thickness of the order of 10 μm: this suggests that a two-dimensional mathematical modeling of the system could be sufficient to capture the main characteristics of the phenomenon.

Remark. In order to roughly estimate the depth into the ECM thickness at which the superficial action of the cells is influential, we observe that the main balance is between the cell traction τ and the shear stresses τ_{xz}, τ_{yz} of the substratum. Denoting by U the order of magnitude of the horizontal displacement of the cells, and by Z the typical length scale of the vertical displacement of the ECM, we have the relation $\mu U/Z \sim \tau$, that yields in turn

$$Z \sim \frac{\mu U}{\tau},$$

where μ is the Lamé elastic constant of the substratum. From experimental measurements (Galbraith and Sheetz, 1997; Namy et al., 2004), it is known that

$$\mu \sim 10^3 \text{ Pa}, \qquad U \sim 10\ \mu\text{m}, \qquad \tau_{\max} \sim 10^2 \text{ Pa},$$

hence $Z_{\max} \sim 10^2\ \mu$m is obtained. Since this value is much higher than the actual thickness of the substratum used in the experiments mentioned above, we conclude that the action of the cells is not confined in a thin layer under the top surface of the ECM, but it influences the whole thickness of the latter. This observation supports the possibility to adopt a two-dimensional mathematical modeling

[1] http://embojournal.npgjournals.com

of the substratum via an averaging process of the corresponding three-dimensional equations (see below).

We model the biomechanical system illustrated in the previous section as a set of 2 two-dimensional layers that move and stretch over each other, experiencing mutual interaction forces in the horizontal plane. The unknowns of the problem are therefore the horizontal displacement of the substratum $\mathbf{u}(\mathbf{x}, t)$ and the horizontal velocity field of the cells $\mathbf{v}(\mathbf{x}, t)$, associated to a density field $\rho(\mathbf{x}, t)$, where $\mathbf{x} = (x, y)$. In the experimental papers, the cellular density is usually referred to in terms of number of cells per unit area; here, instead, ρ denotes the mass of the cellular matter per unit surface.

The momentum balance for the ECM reads

$$-\nabla \cdot \mathbb{T}_s = \boldsymbol{\sigma}, \tag{1}$$

where $\mathbb{T}_s$ is the (two-dimensional) Cauchy stress tensor of the substratum and $\boldsymbol{\sigma}$ is the force per unit surface occurring between the ECM and the cells.

The mass conservation and the momentum balance equations for the cell density field are given by

$$\frac{\partial \rho}{\partial t} + \nabla \cdot (\rho \mathbf{v}) = 0, \tag{2}$$

$$\frac{\partial}{\partial t}(\rho \mathbf{v}) + \nabla \cdot (\mathbf{v} \otimes \rho \mathbf{v}) - \nabla \cdot \mathbb{T}_c = -\boldsymbol{\sigma} + \rho \mathbf{f}_c. \tag{3}$$

No source is considered at the right-hand side of Eq. (2), the typical time of an experiment being much smaller than the duplication time of the cells. In some experiments possible detachments of the cells from the substratum are reported (Tranqui and Tracqui, 2000), but we disregard them as higher order effects.

The forces appearing in Eq. (3) have a different physical nature: the stress tensor $\mathbb{T}_c$ accounts for internal forces in the cell layer; $\boldsymbol{\sigma}$ is an external force for the cellular layer, that reads as internal for the whole system; the bulk force per unit mass $\mathbf{f}_c$ accounts for cell–cell interaction via the chemotactic signaling.

The first and second terms in the left-hand side of Eq. (3) are formally identical to the usual material acceleration of a continuum. However, this does not mean that cells behave like particles, the Galilean inertia being definitely negligible in this context. Rather, the nonlinear term at the left-hand side of Eq. (3) accounts for persistence in cell motion, i.e., for their "inertia" in changing their direction (Friedl and Wolf, 2003; Sambeth and Bamgaertner, 2001). Far from claiming that this is the unique way to model persistence in a continuous modeling of the cellular matter, we just remark that persistence is an essential ingredient to design a mathematical model of cell networking, and this is a possible choice that works.

The chemotactic interaction is introduced in the present context as a surface force that tends to aggregate the cells, driving them along the direction of the chemical gradient:

$$\mathbf{f}_c = \beta \nabla c.$$

Furthermore, the balance of the chemotactic factor, characterized by the concentration field per unit volume $c(\mathbf{x}, t)$, is governed by a standard reaction-diffusion

equation

$$\frac{\partial c}{\partial t} - D\Delta c = \alpha(\rho)\rho - \frac{c}{\tau},$$

where D is the diffusion coefficient. The quantities τ and $\alpha(\rho)$ are the half-life and the production rate of the chemoattractant factor and are due to the degradation process and the production by cells, respectively. In this paper, we assume that long-range chemotactic communication is switched off when cells reach an aggregate state; therefore, the function $\alpha(\rho)$ should be characterized by the following properties:

(i) a finite maximum for $\rho = 0$ and a monotone decreasing behavior for $\rho > 0$, in order to mimic the diminishing in the chemoattractant production as the cellular matter becomes more aggregate;
(ii) $\alpha(\rho) \to 0$ when $\rho \to +\infty$ rapidly enough in order for the chemoattractant production to vanish when cells come in a sufficiently packed configuration.

3.1. Mechanical constitutive equations

The extracellular matrix is known to exhibit a viscoelastic mechanical behavior, characterized by relaxation times of the order of 100 s at most. Therefore, in the present context, dealing with a process that lasts hours, we can straightforwardly neglect the viscoelastic effects and suppose that the Cauchy stress tensor depends on the strain tensor:

$$\mathbb{T}_s = \mathbb{T}_s(\nabla \mathbf{u}). \tag{4}$$

In particular, in the following we assume that the displacement of the ECM is sufficiently small that linear elasticity applies. Note that because of the previously mentioned two-layers hypothesis, Eqs. (1) and (4) have to be understood within the framework of a plane problem of elastostatics, assuming in particular a state of *plane stress*. Regarding the analytical derivation of the proper equations for such a problem in terms of the displacement $\mathbf{u}$ of the substratum[2], we specifically refer to Gurtin (1972).

The cellular layer has been effectively modeled in other papers as an elastic fluid (Ambrosi et al., 2004; Gamba et al., 2003; Serini et al., 2003):

$$\mathbb{T}_c = -p(\rho)\mathbb{I},$$

where $\mathbb{I}$ is the identity 2×2 matrix, and $p(\rho)$ is a function such that its gradient is negligible for small density and strongly increases when a density near to the close packing of the cells is approached.

[2] As a matter of fact, the analytical derivation of the equilibrium equations for a linear elastic plane stress problem involves an averaging process of the corresponding three-dimensional equations along the thickness of the substratum. Therefore, $\mathbf{u}$ should be more correctly interpreted as the *average* horizontal displacement of the ECM.

The interaction force $\boldsymbol{\sigma}$ between the cell layer and the ECM drives the deformation of the latter. It is not yet clear which mechanism activates the strong cell adhesion on the ECM that causes the motion to switch from amoeboid to mesenchymal. At the present stage, we can just conjecture that amoeboid motion stops when cells come in "sufficient" contact, i.e., when the network stretch starts up. If at a given time a cell anchors at a point $\mathbf{x}_0$ of the substratum and then moves to $\mathbf{x}_1$, while the substratum is simultaneously stretched so as the point $\mathbf{x}_0$ moves to $\mathbf{x}_2$, a force between the cell and the substratum arises, that we can assume elastic and in particular proportional to $\mathbf{x}_2 - \mathbf{x}_1 = \mathbf{u} - \mathbf{u}_c$, where $\mathbf{u} = \mathbf{x}_2 - \mathbf{x}_0$ and $\mathbf{u}_c = \mathbf{x}_1 - \mathbf{x}_0$. This ideally means that the cell and the ECM are connected by a spring that obeys the linear Hooke's law, $\mathbf{x}_2 - \mathbf{x}_1$ being its elongation (Fig. 1d). Then, we set

$$\boldsymbol{\sigma} = -\kappa(\rho)\,(\mathbf{u} - \mathbf{u}_c)\,, \tag{5}$$

where $\kappa(\rho)$ vanishes for low density. According to Eq. (5), the cells stick to the substratum at the initial time, quite a rough modeling of the real transition from amoeboid to mesenchymal motion observed in the experiments. We just remark that this unsatisfactory modeling point is not a mathematical flaw, rather it is due to a still incomplete biological knowledge.

The reader is referred to the Appendix for the specific form of the functions $p(\rho)$, $\kappa(\rho)$ used in the numerical simulations, as well as of the function $\alpha(\rho)$ introduced above.

4. Discussion of the mathematical model

The balance equations and the constitutive equations stated in Section 3 yield the following differential system:

$$\frac{\partial \rho}{\partial t} + \nabla \cdot (\rho \mathbf{v}) = 0, \tag{6}$$

$$\frac{\partial}{\partial t}(\rho \mathbf{v}) + \nabla \cdot (\mathbf{v} \otimes \rho \mathbf{v}) + \nabla p(\rho) = \kappa(\rho)\,(\mathbf{u} - \mathbf{u}_c) + \beta \rho \nabla c, \tag{7}$$

$$-\frac{E}{2(1+\nu)}\Delta \mathbf{u} - \frac{E}{2(1-\nu)}\nabla(\nabla \cdot \mathbf{u}) = -\kappa(\rho)\,(\mathbf{u} - \mathbf{u}_c)\,, \tag{8}$$

$$\frac{\partial c}{\partial t} - D\Delta c = \alpha(\rho)\rho - \frac{c}{\tau}, \tag{9}$$

where E and ν denote the Young modulus and the Poisson ratio of the substratum, respectively, supplemented by the compatibility condition:

$$\frac{\mathrm{d}\mathbf{u}_c}{\mathrm{d}t} = \mathbf{v}. \tag{10}$$

When $\kappa \equiv 0$ no interaction exists between the layers, the dynamics of ECs and ECM are decoupled, and one partially recovers the chemotactic model by Ambrosi et al. (2004).

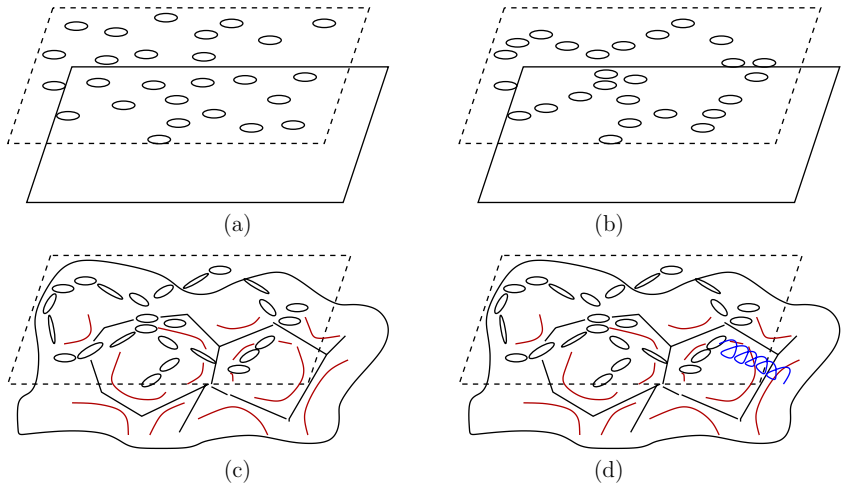

Fig. 1 Random seeding of the cells (a), amoeboid cell migration along the gradient of the chemoattractant concentration (b), traction between the cellular layer and the gel (c). In (d), the spring ideally connecting the two layers is pictorially shown.

The evolution of the system predicted by the set of Eqs. (6)–(10) is depicted in Fig. 1. After the random seeding of the cells (Fig. 1a), the chemotactic field is set up. Cells start moving along the chemical gradient, driven by the chemotactic force (Fig. 1b). The persistence term in the equations makes the cellular matter preserve its initial direction of motion, which is not in general strictly directed toward larger density points. This delay in the cellular response causes cells not to cluster; they instead empty the lower density regions, forming a density pattern with spatial characteristics dictated by the typical length $\ell \approx \sqrt{D\tau}$ (see Ambrosi et al., 2004). The traction between the cellular layer and the gel starts acting when a sufficiently large density is locally obtained, so that $\kappa(\rho)$ is not negligible. At this stage (Fig. 1c), cells hang on and stretch the substratum. In Fig. 1d is pictorially shown the spring ideally connecting the two layers. Cell–ECM adhesiveness and mechanical characterization of the substratum are two distinct physical effects that are duly incorporated into the model by different terms. The function $\kappa(\rho)$ accounts for adhesiveness, a mutual characterization of cells and ECM; on the other hand, E and ν measure the stiffness of the material composing the substratum.

The final scenario can be understood by summing up Eqs. (7) and (8) at the steady state, after obtaining c formally from Eq. (9):

$$-\frac{E}{2(1+\nu)}\Delta\mathbf{u} - \frac{E}{2(1-\nu)}\nabla(\nabla\cdot\mathbf{u}) + \nabla p(\rho) = \\ = \beta D\rho\nabla\left[\left(\frac{1}{D\tau} - \Delta\right)^{-1}\alpha(\rho)\rho\right]. \tag{11}$$

If the system is far from the percolative transition threshold (low ρ), the intercellular pressure is negligible and Eq. (11) accounts for the balance between the aggregative tendency of the anchored cells (right-hand side) and the elastic

response of the ECM (left-hand side). The non-local operator at the right-hand side of Eq. (11) acts as a filter, damping the wavelengths larger than $\sqrt{D\tau}$ (see Ambrosi et al., 2004).

Equation (11) is very similar to the force balance equation written by Manoussaki and coworkers (Manoussaki et al., 1996) for the gel–cell system. Their seminal work has pioneered a class of mathematical models (see also Manoussaki, 2003; Namy et al., 2004) describing the in vitro vasculogenesis in terms of mechanical interactions between ECs and ECM. In the following, we shall briefly sketch the main analogies and differences between these models and the general formulation illustrated in the present paper.

(i) Manoussaki and coworkers do not write a differential equation for the velocity $\mathbf{v}$ of the cells, and therefore they do not account for persistence. In their model, the movement of the cells is due to the superposition of a diffusive "matrix guided" motion (a movement biased toward the directions of the principal strains of the ECM), and the drift velocity $\frac{\partial \mathbf{u}}{\partial t}$. Namy and coworkers (Namy et al., 2004) add to this framework some other more sophisticated effects, such as cell sensitivity to ECM density gradient (*haptotaxis*) and long-range interactions in ECM stretching due to the fibrous nature of the substratum.

(ii) The models presented in Manoussaki (2003), Manoussaki et al. (1996), and Namy et al. (2004) consider the spatial reorganization of the ECM mass induced by cellular tractions as one of the main factors for the formation of the networks; consequently, they all include a balance equation for the ECM density, a quantity that plays no specific role here.

(iii) Manoussaki and coworkers write a force balance equation for the gel–cell system very similar to Eq. (11), including the shear stress of the Petri dish on the ECM. We do not explicitly take into account this contribution, but we recover otherwise its main effect, which essentially consists in filtering out the rigid motion of the gel (see Section 5).

(iv) In general, chemotaxis and all the related effects are completely neglected. Actually, Manoussaki (2003) acknowledges a theoretical role to chemotactic factors, and indeed she includes them in her model by a diffusion equation analogous to Eq. (9); however, they are disregarded in the numerical simulations. Note that if no diffusion of chemoattractant occurs, then the non-local operator at the right-hand side of Eq. (11) disappears and the density field ρ directly drives the stretch of the ECM, without the *filtering* operated by the chemical field. No characteristic length independent of the initial conditions should then be observed in such a case.

5. Quantitative results

The model illustrated in the previous sections has been converted in a dimensionless form (see Appendix), and then numerically integrated in the reference square with a spatial resolution of 128×128 nodes. Numerical simulations have been performed using this set of non-dimensional parameters and

functions:

$$\nu = 0.2, \qquad \beta^* = 0.02, \qquad \eta^* = 50$$

$$\kappa^*(\rho^*) = 0.2\rho^*, \qquad \alpha^*(\rho^*) = \frac{30}{1 + 0.2\rho^{*2}}.$$

Periodic boundary conditions have been prescribed for all the state variables; furthermore, the following non-dimensional initial conditions have been imposed:

$$\rho^*(\mathbf{x}^*,\, 0) = \frac{1}{2\pi r^{*2}} \sum_{j=1}^{M} \exp\left(-\frac{|\mathbf{x}^* - \mathbf{x}_j^*|^2}{2r^{*2}}\right),$$

$$\mathbf{v}^*(\mathbf{x}^*,\, 0) = \mathbf{u}^*(\mathbf{x}^*,\, 0) = c^*(\mathbf{x}^*,\, 0) = 0.$$

The initial condition on the cellular density corresponds to a set of M Gaussian bumps whose amplitude is assumed to be of the order of the non-dimensional average cell radius r^* (the physical cell radius being about $r = 20\,\mu$m), centered randomly in $\mathbf{x}_j^*$, $j = 1, \ldots, M$, with a uniform distribution over the square.

After an implicit discretization in time by a backward Euler scheme, the parabolic Eq. (9) has been discretized in space by a spectral method and solved by the Fast Fourier Transform algorithm. The elliptic non-evolutive Eq. (8) has been discretized by a spectral method nested in an iterative procedure to take into account the spatially non-constant coefficient term $-\kappa(\rho)\mathbf{u}$ at the right-hand side. Note that the presence of periodic boundary conditions on $\mathbf{u}$ causes the substratum not to be constrained in any way. Rigid motions are removed from the set of possible motions by imposing that the amplitude of the Fourier mode corresponding to the null wavenumber vanishes. Equations (6) and (7) constitute a nonlinear hyperbolic system with source term; the right-hand side has been discretized by a Godunov method, while a simple centered discretization has been applied to the left-hand side. The displacement field of the cells $\mathbf{u}_c$ (Eq. (10)) is numerically obtained integrating in time the velocity field $\mathbf{v}$ by a first-order finite difference scheme.

Figure 2 shows a comparison between the experimental pictures of the vascular network formation as obtained by videomicroscopy (a) and as predicted by the model (b). The non-dimensional time is listed in the left column. The geometrical properties of the network shown in Fig. 2b are very similar to the experimentally observed ones.

Figure 3 shows the influence of cellular adhesiveness to the substratum on the formation of vascular networks as predicted by the model. If the adhesiveness is too strong, no network forms (Fig. 3c). As the adhesiveness is the macroscopic result of microscopic chemical bonds that occur between each cell and the ECM, the stronger the bonds are, the more inhibited the movement of the cells is. On the other hand, for too weak adhesiveness the chemotactic action becomes prevalent, and one can observe a rapid formation of cords that do not reach a steady state (Fig. 3b), like in the mathematical model proposed by Ambrosi et al. (2004): cells

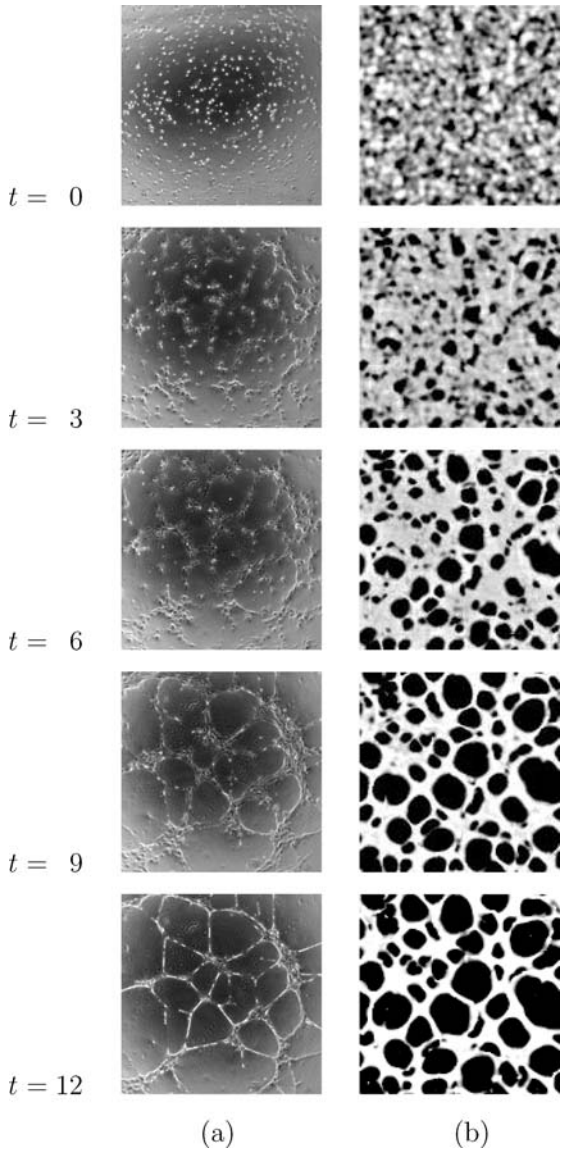

Fig. 2 Formation of capillary networks: Comparison between the experimentally observed (a) and the numerically predicted (b) morphology. The experimental pictures refer to a density of 125 cells/mm^2 of human microvascular ECs on a 4 mm^2 wide portion of Matrigel. Accordingly, the numerical simulation has been carried out starting from an initial condition of the form given in § 5 with $M = 800$, which closely mimics the real cell density. Numerical integration of the initial condition over the reference square allows to easily verify this claim, considering that the average cell mass is about 3×10^{-11} kg. The non-dimensional time listed in the left column can be straightforwardly converted in dimensional form using the characteristic time $\tau = 1$ h.

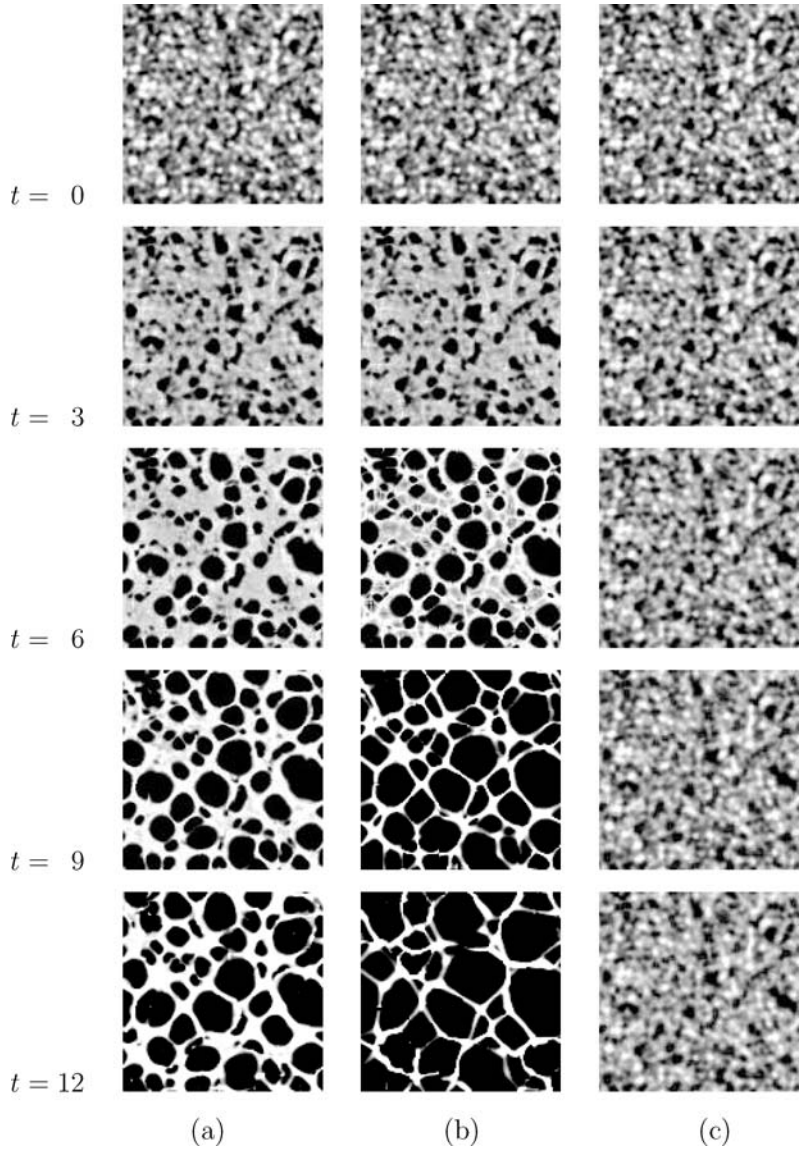

Fig. 3 Influence of cellular adhesiveness to the substratum on network formation. When chemotactic attraction and mechanical interactions balance, a stable network structure arises (a). Instead, if adhesiveness is too low (b) or too strong (c) cords either rapidly form without giving rise to a stable structure or they do not form at all.

continue to pack and they finally cluster in big mounds. Only when chemotactic attraction and mechanical interactions balance does a stable network structure form (Fig. 3a). In particular, numerical simulations show that the networking is essentially allowed or inhibited by the relative magnitude of the parameters

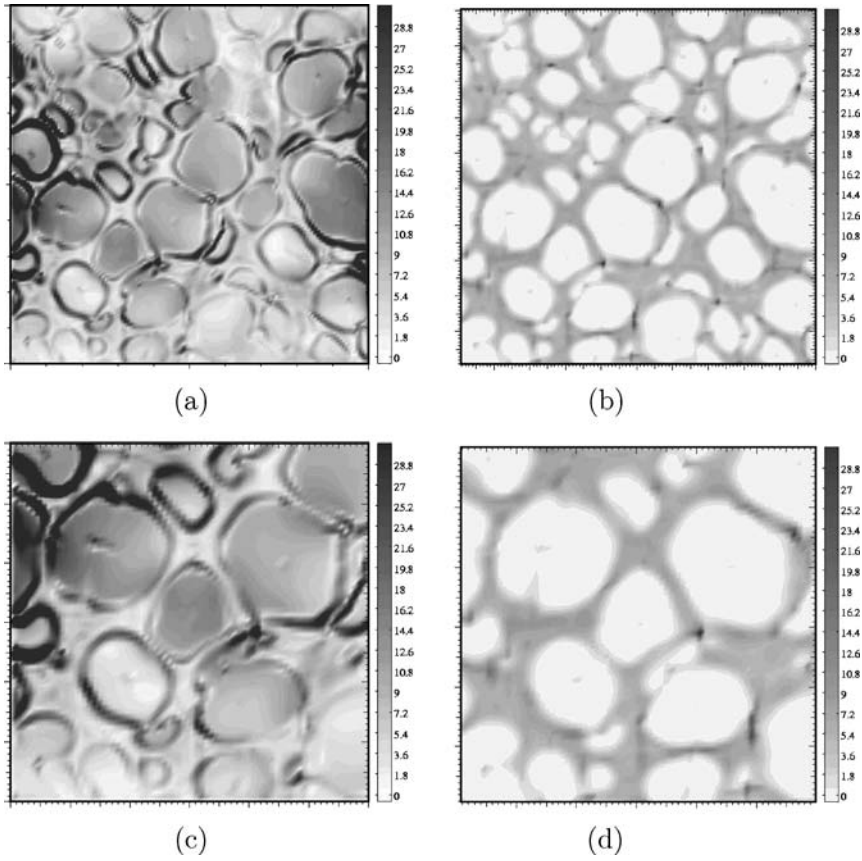

Fig. 4 Plot of the norm of the ECM stress tensor (a) and the corresponding ECs density (b) at the final stage of network formation. A magnification of a portion of the domain is also shown (c and d). Stress values are here reported in dimensional form (obtained using $\nu = 0.2$ and $E = 10^3$ Pa as in Namy et al., 2004), corresponding to a maximum value of about 30 Pa.

β^* and κ^*, that, up to non-dimensionalization, account for the intensity of the intercellular chemotactic signaling and for the stiffness of the ECs–ECM adhesion, respectively. Conversely, the morphogenetic process is virtually independent of the Young modulus E of the substratum, which instead affects mainly the magnitude of the ECM deformation and displacement from the unstressed configuration (see Appendix).

As mentioned in Section 2, at later times cells differentiate in tubular structures and, consequently, the present two-dimensional model no longer applies. Figure 4a shows the contour plot of the ECM stress tensor norm $\|\mathbb{T}_s\|$ at the final stage of the network formation, the corresponding cellular density being represented in Fig. 4b. We use the definition

$$\|\mathbb{T}_s\|^2 := \text{trace}\left(\mathbb{T}_s^T \mathbb{T}_s\right),$$

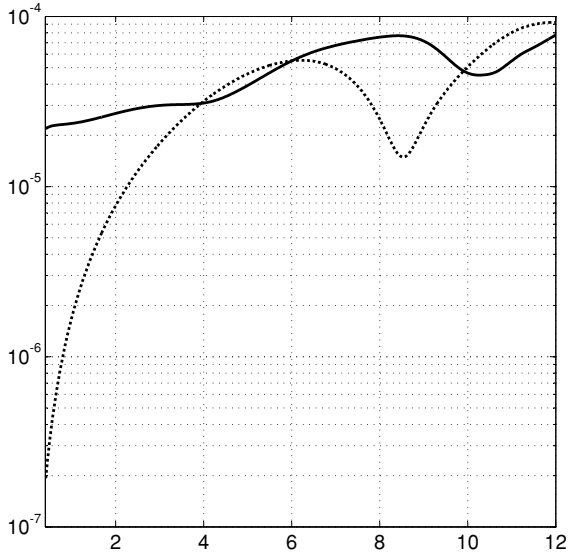

Fig. 5 Plot in semi-logarithmic scale of the magnitude of the spatially averaged chemotactic (*solid line*) and elastic (*dotted line*) forces vs. time.

so that $\|\mathbb{T}_s\|$ gives a measure of the magnitude of the stress affecting the substratum due to the traction exerted by the cells. Figure 4c and d are magnifications of the previous pictures referred to a particular area of the domain. Numerical simulations suggest that most stress is concentrated in thin strips edging the cords or surrounding the cell density holes. In Fig. 5, the magnitude of the spatially averaged chemotactic and elastic forces are compared. The plot shows that in the early times of the simulation the chemotactic force grows more rapidly than the elastic one, so that in the first period (say about $0 \leq t \leq 3$) chemotaxis dominates. Later the elastic force grows, until a substantial equilibrium is reached.

6. Final remarks

This paper is based on the observation that, in vascular network formation, migration and traction are different programs that an individual cell is able to execute. We conjecture that the beginning of either program is dictated by the local cell density, which leads the system to an amoeboid or mesenchymal regime.

In our opinion, persistence, chemotaxis, and mechanics provide complementary description of in vitro vasculogenesis experiments. Persistence and endogenous chemotaxis are essential ingredients in the early, migration-dominated stages of network formation. They govern the size of the capillary structure via the diffusion coefficient D and the chemoattractant half-life τ. The predicted average size of the fully formed network structures is $\ell \approx \sqrt{D\tau}$, in good agreement with phenomenological observations in vivo and measurements in vitro. Intriguingly, this

is in agreement with the observation that mice lacking heparin-binding isoforms of VEGF-A, characterized by smaller diffusivity, form vascular networks with a larger mesh (Ruhrberg et al., 2002).

The main role of the mechanical interactions between ECs and ECM is to stabilize the structures. In the purely chemotactic model by Ambrosi et al. (2004), the cell–cell interaction is confined to normal stresses only, given by the intercellular pressure $p(\rho)$. Although this is a sufficient condition in order for the solution $\rho(\mathbf{x}, t)$ not to blow-up in time, as proved by Kowalczyk (2005), it does not guarantee the preservation of the network morphology under shear perturbations. Instead, the anchorage of the cells to the substratum, which is able to sustain not only normal stress but also shear stress, provides stability to the structures.

Of course, some issues remain to be investigated in the future. For instance, some experimental movies show that the ECM can be locally stretched at a high ratio, including not negligible vertical displacements. This behavior would prevent from using a linear elastic model, and also the "thin layer" approximation could not apply.

A natural generalization of the present work would be to extend the mathematical model to three-dimensional cell migration. Unfortunately, recent experimental investigations suggest that a pure transposition of the theory would be just an academic exercise. In fact, three-dimensional migration of the cells occurs in a very different way (Friedl and Wolf, 2003; Wolf et al., 2003): Cells essentially thread themselves and climb fibers of the ECM. The motion is always mesenchymal, and fibers orientation plays a fundamental role. It remains an open question to what extent the achievements in the understanding of the two-dimensional vasculogenesis will be helpful to address the real three-dimensional setting.

Acknowledgements

This work has been funded by the FIRB project RBAU01K7M2 "Metodi dell'analisi matematica in biologia, medicina e ambiente" and the MC-RTN Project MRTN-CT-2004-503661 "Modelling, mathematical methods and computer simulation for tumour growth and therapy".

Appendix: Non-dimensional form of the equations

Let us introduce the following non-dimensional variables:

$$\mathbf{x}^* := \frac{\mathbf{x}}{\ell}, \qquad t^* := \frac{t}{T}, \qquad \rho^* := \frac{\rho}{\rho_0}, \qquad c^* := \frac{c}{C}$$

where ℓ, T, ρ_0, C are typical values of length, time, cell density, and chemoattractant concentration, respectively.

Choosing $\ell = \sqrt{D\tau}$ (as suggested by Eq. (9) at the steady state) and $T = \tau$ yields the non-dimensional system

$$\frac{\partial \rho^*}{\partial t^*} + \nabla^* \cdot (\rho^* \mathbf{v}^*) = 0$$

$$\frac{\partial}{\partial t^*}(\rho^* \mathbf{v}^*) + \nabla^* \cdot (\mathbf{v}^* \otimes \rho^* \mathbf{v}^*) + \nabla^* p^*(\rho^*) = \kappa^*(\rho^*)(\mathbf{u}^* - \mathbf{u}_c^*) + \beta^* \rho^* \nabla^* c^*$$

$$-\Delta^* \mathbf{u}^* - \frac{1+\nu}{1-\nu}\nabla^*(\nabla^* \cdot \mathbf{u}^*) = -\eta^* \kappa^*(\rho^*)(\mathbf{u}^* - \mathbf{u}_c^*)$$

$$\frac{\partial c^*}{\partial t^*} - \Delta^* c^* = \alpha^*(\rho^*)\rho^* - c^*,$$

where we have defined the following non-dimensional groups of parameters:

$$\beta^* := \frac{\beta C \tau}{D}, \qquad \eta^* := \frac{2(1+\nu)\rho_0}{E\tau^2}$$

and the following non-dimensional functions:

$$p^*(\rho^*) := \frac{\tau}{D\rho_0} p(\rho_0 \rho^*), \qquad \kappa^*(\rho^*) := \frac{\tau^2}{\rho_0}\kappa(\rho_0\rho^*), \qquad \alpha^*(\rho^*) := \frac{\rho_0 \tau}{C}\alpha(\rho_0\rho^*).$$

If ρ_0 is thought of as the close-packing cell density, a possible intercellular pressure that behaves as described in Section 3 is

$$p^*(\rho^*) = \begin{cases} \epsilon\rho^* & \text{for } 0 \le \rho^* \le 1 \\ \epsilon\rho^* + b(\rho^* - 1)^3 & \text{for } \rho^* > 1 \end{cases} \qquad 0 < \epsilon \ll 1,\ 0 \le b \ll 1$$

or, with weaker requirements on the regularity of the function p^*,

$$p^*(\rho^*) = \begin{cases} \epsilon\rho^* & \text{for } 0 \le \rho^* \le 1 \\ \epsilon + b(\rho^* - 1) & \text{for } \rho^* > 1 \end{cases}$$

and in this case $0 < \epsilon < b \ll 1$.

Moreover, we choose for $\kappa^*(\rho^*)$ a simple linear dependence on ρ^*:

$$\kappa^*(\rho^*) = \kappa^* \rho^*, \qquad \kappa^* > 0,$$

which actually implies a constant adhesiveness κ^* between ECs and ECM, and an elastic force proportional to the cell density.

Finally, according to the dynamics described in Section 3 (hypotheses (i) and (ii)), we use for $\alpha^*(\rho^*)$ the following expression:

$$\alpha^*(\rho^*) = \frac{\alpha_1}{1 + \alpha_2 \rho^{*2}}$$

with $\alpha_1 > 0$ and $\alpha_2 \geq 0$. Consequently, the production rate of chemoattractant is nearly independent of the cell density for low ρ^* and essentially vanishes for $\rho^{*2} \gg \frac{1}{\alpha_2}$.

Remark. Experimental measurements (see e.g., Serini et al., 2003) indicate that the order of magnitude of the diffusion coefficient of the chemical factor is $D \sim 10^{-7}$ cm^2/s, while its half-life is $\tau \sim 1$ h; consequently, the characteristic length ℓ turns out to be about 200 μm, in good agreement with the characteristic cord length experimentally observed.

Moreover, in order to estimate the parameter ρ_0 we assume that the close-packing cell density corresponds to the idealized situation in which each EC gets in touch with four other neighboring cells without overlapping. Here, we specifically refer to the experimental assay by Serini et al. (2003). Geometrically, regarding ECs as circles of constant radius, this configuration leads to a portion of plane surface covered by cells amounting to about 78% of the total surface of the ECM, which in turn implies for ρ_0 an order of magnitude of 2×10^{-2} kg/m^2.

Finally, direct measurements of the parameter β, that in the model drives the networking via the chemotactic signaling, are not available. However, an indirect tuning of its non-dimensional counterpart β^* is possible on the basis of the total time (12–15 h) needed for a complete formation of the structures.

References

Ambrosi, D., Gamba, A., Serini, G., 2004. Cell directionality and chemotaxis in vascular morphogenesis. Bull. Math. Biol. 66(6), 1851–1873.

Ambrosi, D., Bussolino, F., Preziosi, L., 2005. A review of vasculogenesis models. J. Theor. Med. 6(1), 1–19.

Bischofs, I.B., Schwartz, U.S., 2003. Cell organization in soft media due to active mechanosensing. PNAS, 100, 9274–9279.

Friedl, P., Wolf, K., 2003. Tumour-cell invasion and migration: Diversity and escape mechanisms. Nat. Rev. Cancer 3, 362–374.

Ferrenq, I., Tranqui, L., Vailhe, B., Gumery, P.Y., Tracqui, P., 1997. Modelling biological gel contraction by cells: Mechanocellular formulation and cell traction quantification. Acta Biotheor. 45, 267–293.

Gamba, A., Ambrosi, D., Coniglio, A., de Candia, A., Di Talia, S., Giraudo, E., Serini, G., Preziosi, L., Bussolino, F., 2003. Percolation, morphogenesis and Burgers dynamics in blood vessels formation. Phys. Rev. Lett. 90, 11810/1–4.

Galbraith, G.G., Sheetz, M.P., 1997. A micromachined device provides a new bend on fibroblast traction forces. PNAS Cell Biol. 94, 9114–9118.

Gazit, Y., Berk, D.A., Leunig, M., Baxter, L.T., Jain, R.K., 1995. Scale-invariant behavior and vascular network formation in normal and tumor tissue. Phys. Rev. E 75, 2428–2431.

Grant, D., Tashiro, K., Segui-Real, B., Yamada, Y., Martin, G., Kleinman, H., 1989. Two different laminin domains mediate the differentiation of human endothelial cells into capillary-like structures in vitro. Cell 58, 933–943.

Gurtin, M.E., 1972. The linear theory of elasticity. In: Flügge, S. (Ed.), Handbuch der Physik, Vol. VI a/2. Springer Verlag, Berlin.

Helmlinger, G., Endo, M., Ferrara, N., Hlatky, L., Kain, R.K., 2000. Formation of endothelial cell networks. Nature 405, 139–141.

Hendrix, M.J.C., Seftor, E.A., Meltzer, P.S., Gardner, L.M.G., Hess, A.R., Kirschmann, D.A., Sachatteman, G.C., Seftor, R.E.B., 2001. Expression and functional significance of VE-cadherin in aggressive human melanoma cells: Role in vasculogenic mimicry. Proc. Natl. Acad. Sci. USA 98, 8018–8024.

Kubota, Y., Kleinman, H., Martin, G., Lawley, T., 1988. Role of laminin and basement membrane in the morphological differentiation of human endothelial cells into capillary-like structures. J. Cell Biol. 107, 1589–1598.

Kowalczyk, R., 2005. Preventing blow-up in a chemotaxis model. J. Math. Anal. Appl. 305, 566–588.

Manoussaki, D., 2003. A mechanochemical model of angiogenesis and vasculogenesis. ESAIM: Math. Model. Num. Anal. 37(4), 581–600.

Manoussaki, D., Lubkin, S.R., Vernon, R.B., Murray, J.D., 1996. A mechanical model for the formation of vascular networks in vitro. Acta Biotheor. 44, 271–282.

Mariotis, A.J., Folberg, R., Hess, A., Seftor, E.A., Gardner, L.M.G., Pe'er, J., Trent, J.M., Meltzer, P.S., Hendrix, M.J.C., 1999. Vascular channel formation by human melanoma cells in vivo and in vitro: Vasculogenesis mimicry. Am. J. Pathol. 155, 739–752.

Murray, J.D., Oster, G.F., 1984. Cell traction models for generation of pattern and form in morphogenesis. J. Math. Biol. 19, 265–279.

Namy, P., Ohayon, J., Tracqui, P., 2004. Critical conditions for pattern formation and in vitro tubulogenesis driven by cellular traction fields. J. Theor. Biol. 227, 103–120.

Ruhrberg, C., Gerhardt, H., Golding, M., Watson, R., Ioannidou, S., Fujisawa, H., Betsholtz, C., Shima, D., 2002. Spatially restricted patterning cues provided by heparin-binding VEGF-A control blood vessel branching morphogenesis. Gen. Dev. 16, 2684–2698.

Serini, G., Ambrosi, D., Giraudo, E., Gamba, A., Preziosi, L., Bussolino, F., 2003. Modeling the early stages of vascular network assembly. EMBO J. 22, 1771–1779.

Sambeth, R., Bamgaertner, A., 2001. Autocatalytic polymerization generates persistent random walk of crawling cells. Phys. Rev. Lett. 86, 5196–5199.

Tranqui, L., Tracqui, P., 2000. Mechanical signalling and angiogenesis. The integration of cell-extracellular matrix couplings. C.R. Acad. Sci. Paris, Science de la Vie 323, 31–47.

Vailhe, B., Vittet, D., Feige, J.J., 2001. In vitro models of vasculogenesis and angiogenesis. Lab. Invest. 81, 439–452.

Webb, D.J., Horwitz, A.F., 2003. New dimensions in cell migration. Nat. Cell Biol. 5, 690–692.

Wolf, K., Mazo, I., Leung, H., Engelke, K., von Andrian, U.H., Deryugina, E.I., Strongin, A.Y., Bröcker, E.-B., Friedl, P., 2003. Compensation mechanism in tumor cell migration: Mesenchymal-amoeboid transition after blocking of pericellular proteolysis. J. Cell Biol. 160, 267–277.